

A MULTI-DIMENSIONAL ADAPTIVE SAMPLING METHOD FOR ANALYSIS AND DESIGN OF FREQUENCY SELECTIVE SURFACE WITH ARBITRARY ELEMENT

X. Ma^{*}, G.-B. Wan, and W. Wan

School of Electronics and Information, Northwestern Polytechnical University, Xi'an, Shaanxi 710129, China

Abstract—A fast and efficient multi-dimensional adaptive sampling method (ASM) based on Stoer-Bulirsch (S-B) algorithm for frequency selective surface (FSS) analysis and design is presented in this paper. The multivariate rational function is established according to the functional relation of the scattering parameters with frequency and direction of incident wave, medium parameters and geometry dimensions of FSS structure, et al.. In order to evaluate the values of the multivariate rational function fully automatically without determining the coefficients of the targeted rational interpolant, the one-dimensional S-B algorithm is expanded into multidimensional method. The sampling points in each dimension are chosen at the areas of maximum error in an adaptive way. The recursive interpolation results of one dimension are used as the initial values of next dimension in the recursive tabular until n th-dimensional recursive interpolation is accomplished. The initial values of recursive algorithm are calculated by spectral domain method of moments (MoM) at every sample point. The current distribution of FSS cell is predicted by Rao-Wilton-Glisson (RWG) subdomain basis functions which are applicable for arbitrarily shape elements. Four examples, including FSS with the eight-legged, cross and ring elements and FSS radome enclosed antennas, are considered to demonstrate the feasibility of applying the multi-dimensional ASM to analysis and optimal design of FSS. Numerical results show that the proposed method is superior in computation efficiency compared to the direct MoM. Good agreement between the proposed technique and the direct MoM is observed.

Received 20 April 2012, Accepted 27 May 2012, Scheduled 4 June 2012

* Corresponding author: Xin Ma (maxin1105@yahoo.com.cn).

1. INTRODUCTION

The FSS which consists of a periodic array have been the subject of extensive studies [1–9] in recent years owing to its capability of spatial filters in widespread application. The classic examples of these applications are radar antennas radome in stealth technology and subreflector in multiband communication. Therefore, more attention has been paid to numerical method to the treatment of FSS and the angular stability, complex structure of FSS [1, 2]. Among various numerical methods, the most popular technique [3] is the MoM. The RWG subdomain basis function [4] has been used for arbitrary shape geometry of FSS cell [5], in which the RWG basis function is uniform discretization which limits the flexibility of modeling the complex geometry.

When the structure of FSS is large relative to wavelengths of interest, the direct MoM often results in large matrices that can be very time-consuming to solve. It is more preferred to employ an iterative procedure, e.g., the conjugate gradient method (CGM) [5] or multilevel fast multiple algorithm (MFMA) [6]. With the increasing complexity of applications and design of FSS, it is often needed to do the calculations at finer increment to obtain an accurate representation of the response over a broad frequency or incident angle range [7]. There is a strong desire to find approximate solution techniques to eliminate repetition computation. One effective method is using the rational function to interpolate the required data by model-based functions.

Various methods have been proposed to establish appropriate rational function. The asymptotic waveform evaluation (AWE) technique has been used in various electromagnetic problems [10]. It is found to be superior in terms of the CPU time to obtain frequency response. But the accuracy is limited by the radius of convergence and the high derivatives of the dense impedance matrix must be stored that will result in consuming great memory. The Maehly approximation which is efficient without increasing any memory and computing time, has already successfully used in the scattering analysis of arbitrarily shaped objects [11] and FSS [12] over a broad frequency band. However, the numerical error is always caused with the large number of samples because of the resultant ill-conditioned coefficient matrix whose inverse is inevitable to determine the coefficient of rational function. The general S-B algorithm is employed in adaptive frequency sampling scheme (S-B AFS) for analyzing the scattering characteristic of a general microwave circuit [13] and FSS [14] over a broad bandwidth. The S-B AFS is a recursive tabular method and requires no matrix inversion. Therefore, it can process a large

number of sampling data without suffering from singularity problems and effectively estimates the orders of the required rational function. The S-B AFS greatly simplifies the traditional AFS process, but it is only applicable to frequency response. Only a few multivariate sampling algorithms have been published. For multidimensional cases Lehmsiek and Meyer used a Thiele-type branched continued fraction for microwave circuits [15]. The multidimensional parameterized analytical models which cover whole parameter and frequency space for general planar microwave structures are presented in [16]. In [17], Peik et al. extend the one-dimensional Cauchy method for frequency-response interpolation to a multidimensional Cauchy interpolation, with respect to both frequency and physical dimensions.

In this paper, the S-B AFS algorithm is expanded into multivariate adaptive sampling method to analyze the electromagnetic characteristics of FSS for multi-dimensional parameter space. The current distribution of FSS cell is predicted by RWG basis functions for arbitrarily shape elements. In conjunction with MoM, the multi-dimensional interpolation starts with low-order interpolant. The technique systematically increases the order by optimally choosing new sampling points of each dimension in the areas of highest error. The algorithm converges until the desired accuracy is reached. Sufficient required knowledge has been acquired for rational function interpolation. Employment of adaptive sampling schemes reduces the required number of samples without oversampling the interpolation space. Using the interpolation results of one dimension as the initial values of next dimension, the final interpolation value of the multivariate rational function can be obtained. The model of multivariate rational function covers the whole parameter and frequency space and can easily be used for analysis and optimization purposes.

2. MODEL AND MOM ANALYSIS OF FSS

An infinite array of perfectly conducting patches with periodicities T_x and T_y in the x , y directions, respectively, resides between l th and $(l+1)$ th ($l = 0, 1, \dots, L$) plane dielectric slab. The FSS is illuminated by a plane incidence from the direction of (θ_i, φ_i) , as shown in Fig. 1.

The induced current on the perfectly conduct is expanded using the RWG basis functions. The electric field integral equation (EFIE) [18] can be discretized into the following linear equation by using MoM. Through application of Galerkin's technique, the EFIE is reduced to a matrix equation

$$[Z_{mn}] \cdot [I_n] = [V_m] \quad (n, m = 1, 2, \dots, N) \quad (1)$$

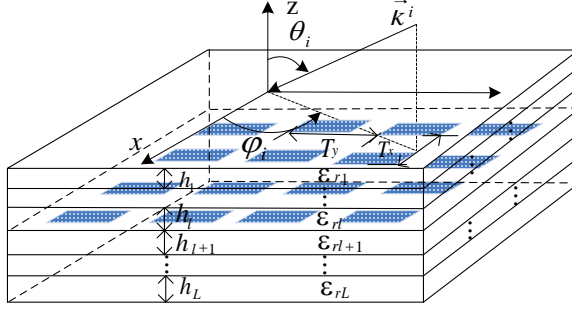


Figure 1. The FSS illuminated by a plane incident wave.

where I_n is unknown coefficient, the elements are expressed as

$$Z_{mn} = \tilde{f}_{xm}^* \tilde{G}_{xx} \tilde{f}_{xn}^* + \tilde{f}_{xm}^* \tilde{G}_{xy} \tilde{f}_{yn}^* + \tilde{f}_{ym}^* \tilde{G}_{yx} \tilde{f}_{xn}^* + \tilde{f}_{ym}^* \tilde{G}_{yy} \tilde{f}_{yn}^* \quad (2)$$

$$V_m = E_x^{\text{inc}} \tilde{f}_{xm}^* + E_y^{\text{inc}} \tilde{f}_{ym}^* \quad (3)$$

where E^{inc} and \tilde{G} represent the incident field and the pertinent dyadic Green's function [18] in the spectral domain, respectively. \tilde{f} denotes the Fourier transforms of RWG basis functions. Referring to [19], it can be represented as

$$\begin{aligned} \tilde{f}^{\pm*} &= f_x^{\pm*} \hat{x} + f_y^{\pm*} \hat{y} \\ &= \pm \frac{l}{2A^\pm} \frac{1}{|k|^2} \sum_{n=1}^3 e^{jkr_{nc}} \left\{ \left[\hat{z} \times L_n + \left(jr_{nc} - j\bar{r} - \frac{2k}{|k|^2} \right) \hat{z} \cdot L_n \times k \right] \right. \\ &\quad \left. j_0 \left(\frac{k \cdot L_n}{2} \right) - L_n \frac{\hat{z} \cdot L_n \times k}{2} j_1 \left(\frac{k \cdot L_n}{2} \right) \right\} \end{aligned} \quad (4)$$

where, $L_n = r_{n+1} - r_n$, $r = x\hat{x} + y\hat{y}$, $k = k_x\hat{x} + k_y\hat{y}$, A^\pm is the area of triangle T^\pm , l is the length of common edge, $*$ denotes the complex conjugate.

Once Eq. (1) is solved, the scattering parameters of FSS can be found rather easily. The reflection coefficients of TE and TM polarization are represented as

$$S^{\text{TE}} = \frac{j(k_{yq}E_x^+ - k_{xp}E_y^+)}{(k_{xp}^2 + k_{yq}^2)} \quad (5)$$

$$S^{\text{TM}} = \frac{(k_{xp}E_x^+ + k_{yq}E_y^+)}{(k_{xp}^2 + k_{yq}^2) \gamma_{pq}/\omega\epsilon} \quad (6)$$

where k_{xp} , k_{yq} and γ_{pq} are the Floquet wavenumber in the x , y and z directions. E^+ is a sum of the reflection fields of the incident

wave through the dielectric structures with all the conducting screens removed and the scattered fields radiated by the conducting screens. More details of the derivation can refer to [18].

3. THEORY OF ADAPTIVE SAMPLING METHOD

The scattering parameters of FSS are related with some variables, for instance the direction of incidence (θ_i, φ_i) , the incident frequency (f) and the parameters of structure (such as geometry dimensions of FSS or the thickness of dielectric slab). These factors can be expressed as vectors $\Pi = (x_1, x_2, \dots, x_n)$ in n -dimensional parameters space and the relationship with scattering parameters can be expressed as a rational function $S(x_1, x_2, \dots, x_n)$. Let x_1 to be f , it is easy to obtain frequency response $S(x_1)$. If x_1 and x_2 are θ_i and φ_i , respectively, it is easy to obtain incident angle response $S(x_1, x_2)$. For traditional MoM, Eq. (1) is required to solve at every finer increment over a broad range. In order to eliminate repetitive computation, the ASM is proposed. Using rational function as interpolation function yields an accurate representation of response with no matrix inversion for unknown coefficients of rational function.

3.1. One-dimensional ASM

For one-dimensional case, a rational function can be defined as [13]

$$S(x_0) = \frac{a_0 + a_1x_0 + \dots + a_\mu x_0^\mu}{b_0 + b_1x_0 + \dots + b_\nu x_0^\nu} \quad (7)$$

where μ and ν are orders of numerator and denominator polynomials. a and b are unknown coefficients which can be obtained by solving a set of linear equations from $\mu + \nu + 2$ samples.

To avoid coefficients matrix inversion, the S-B algorithm of Neville-type [20] is used. The S-B algorithm performs the interpolation on tabular chart in a recurrence manner, as shown in Fig. 2. The value of scattering parameters $S_{i0}(x_{0i})$ calculated by the MoM from Eqs. (5) or (6) at sample x_{0i} is used as the initializing value of the first column in tabular chart. The three different recurrent rules is provided by the S-B algorithm as

$$S_{j,k} = \frac{(x_0 - x_{0,j})S_{j+1,k-1} + (x_{0,j+k} - x_0)S_{j,k-1}}{x_{0,j+k} - x_{0,j}} \quad (8)$$

$$S_{j,k} = \frac{x_{0,j+k} - x_{0,j}}{\frac{x_0 - x_{0,j}}{S_{j+1,k-1}} + \frac{x_{0,j+k} - x_0}{S_{j,k-1}}} \quad (9)$$

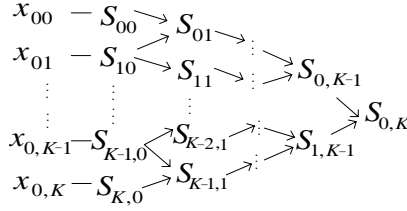


Figure 2. The tabular chart of the S-B algorithm.

$$S_{j,k} = S_{j+1,k-2} + \frac{x_{0,j+k} - x_{0,j}}{\frac{x_0 - x_{0,j}}{S_{j+1,k-1} - S_{j+1,k-2}} + \frac{x_{0,j+k} - x_0}{S_{j,k-1} - S_{j+1,k-2}}} \quad (10)$$

By using a distinct combination of the above three recursive rules in association with a step sequence, an analytical function implemented along a path establishes a rational function model. Based on the recursive rules, the algorithm is organized as follow.

The results recursively calculated corresponding to paths I–III in [13] are defined as three approximate rational function models $S_1(x)$, $S_2(x)$ and $S_3(x)$. Select $S_1(x)$ and $S_2(x)$ as rational function models. Find the sampling point at the areas of highest error ($\max |S_1(x) - S_2(x)|$). When this error is larger than a given error tolerance, the sampling point is added into the sampling collection. Then select $S_2(x)$ and $S_3(x)$ as rational function models and choose the sampling point at the areas of highest error ($\max |S_2(x) - S_3(x)|$). When this error is larger than a given error tolerance, the sampling point is added into the sampling collection. Do the cycle until the convergence error satisfies a termination criterion.

For more details, refer to [13]. The difference between the rational function value S_{ASM} from interpolation and the actual sampling value S_{MOM} from the MoM defines as the convergence error ε

$$\varepsilon = |S_{ASM} - S_{MOM}| / |S_{MOM}| \quad (11)$$

3.2. Multi-dimensional ASM

The multi-dimensional rational function is in the form

$$S(x_1, x_2, \dots, x_n) = \frac{a_0 + \sum_{j=1}^M a_j \left(\prod_{i=1}^n x_i^{\mu_i(j)} \right)}{b_0 + \sum_{j=1}^D b_j \left(\prod_{i=1}^n x_i^{v_i(j)} \right)} \quad (12)$$

where $\mu_i(j)$ and $\nu_i(j)$ are integer functions of j , represent orders of parameters x_i in numerator and denominator polynomials, respectively. a and b are unknown coefficients. $M + D + 2$ samples are required to determine the coefficients of Eq. (12). Once the Eq. (12) is solved, the response $S(x_1, x_2, \dots, x_n)$ can be obtained. The one-dimensional ASM as described in Section 3.1 is extended to a multidimensional ASM to avoid coefficients matrix inversion.

3.2.1. Selecting Sampling Points in an Adaptive Way

Let $[x_i^{\min}, x_i^{\max}]$ denotes the calculating rang of the i th-dimensional parameter. Ψ_i and Φ_i express the set of testing points and the set of sampling points separately in the i th-dimensional parameter space. The testing points x_{it}^{test} ($t = 0, 1, \dots, T_i$) scatter in all range of $[x_i^{\min}, x_i^{\max}]$ with sufficiently fine space. The sampling points must completely fill grid of points which do not have to be equidistant. K_i is the number of sampling points in Φ_i . x_{ik} is the sampling point in Φ_i ($k = 0, 1, \dots, K_i - 1$). The process starts with $K_i = 2$, $x_{i0} = x_i^{\min}$, $x_{i1} = x_i^{\max}$ ($i = 1, 2, \dots, n$). The complete flowchart of the algorithm is given in Fig. 3. More detail of algorithm implementation as follow.

- Step 1: Initialize n th-dimensional parameter space Φ_j and Ψ_j ($j = 1, 2, \dots, n$) and set $i = 1$;
- Step 2: Implement one-dimensional ASM with constant x_s ($s \neq i$) parallel to the x_i -axes;
- Step 3: Find the point at which maximum of error occurs $\epsilon_{\max}(x_{it}^{\text{test}})$;

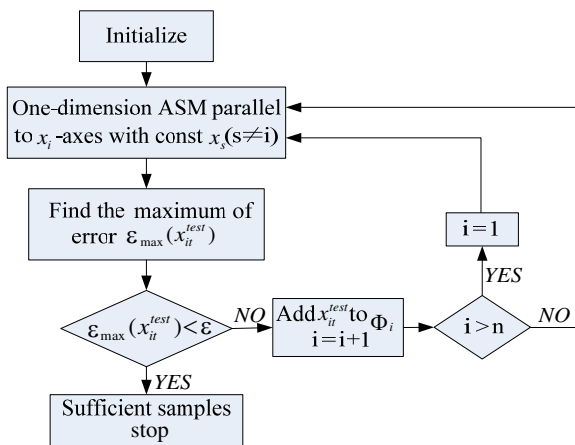


Figure 3. Float chart of multi-dimensional ASM.

- Step 4: By a given error tolerance ε , if $\varepsilon_{\max}(x_{it}^{\text{test}}) < \varepsilon$, the process switches to step 6; otherwise, calculate the value of scattering parameters $S_{\text{MoM}}(x_{it}^{\text{test}})$ at x_{it}^{test} with constant x_s ($s \neq i$) by the MoM, and add point x_{it}^{test} and $S_{\text{MoM}}(x_{it}^{\text{test}})$ to Φ_i ; set $K_i = K_i + 1$, $i = i + 1$;
- Step 5: if $i > n$, set $i = 1$ and go back to step 2; otherwise, go back to step 2 to find the next sample;
- Step 6: Sufficient samples have been acquired for interpolation and all samples have fallen on the grid; K_i is the total number of samples in each dimensional parameter space.

3.2.2. *N*-dimension Recursive Interpolation Method

$S(x_1^*, x_2^*, \dots, x_n^*)$ is the goal to interpolate the rational function value at an arbitrary located point $(x_1^*, x_2^*, \dots, x_n^*)$. The algorithm is divided as following steps.

- Step 1: The samples selected in Section 3.2.1 and the value of scattering parameters calculated by the MoM at these samples are employed as initializing values of interpolation and set $i = 1$;
- Step 2: By using the recursive method, implement one-dimensional interpolation at x_i^* with constant x_s ($s > i$) parallel to the x_i -axes, as shown dashed lines in Fig. 4 for two-dimensional parameter space, and then obtain the transition points $S(x_1^*, x_2, \dots, x_n)$ required for interpolation; set $i = i + 1$;
- Step 3: The transition points of the last interpolation step used as initializing values of the next interpolation step; implement one-dimensional interpolation at x_i^* with constant x_s ($s > i$) parallel to the x_i -axes, and then obtain the new transition points required for the next interpolation; set $i = i + 1$;
- Step 4: Go back to step 3 until $i = n$; implement one-dimensional interpolation at x_n^* parallel to the x_n -axes, as shown dotted lines in Fig. 4 for two-dimensional parameter space, then the target point $S(x_1^*, x_2^*, \dots, x_n^*)$ can be finally got.

4. NUMERICAL RESULTS

To test the accuracy and efficiency of proposed method, the cases of the patch-type eight-legged element FSS, the patch-type cross element FSS and the aperture-type ring element FSS, as shown in Fig. 5, are considered. The multi-dimensional ASM is also applied in calculating the pattern and power transmission of FSS radome enclosed antennas. In the following example, ε is set -80 dB.

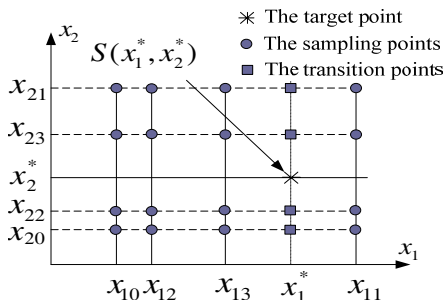


Figure 4. Recursive interpolation method for two-dimensional parameter space.

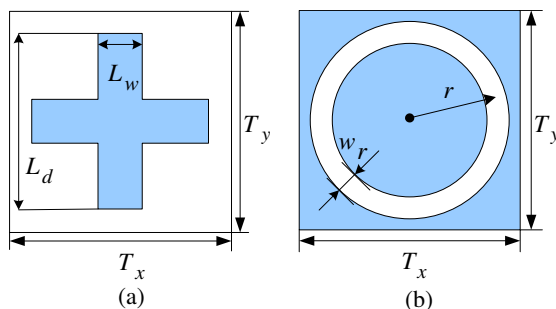


Figure 5. Geometry of FSS cell. (a) Patch-type cross cell. (b) Aperture-type ring cell.

4.1. The Patch-type Eight-legged Element FSS

The eight-legged array is investigated as the first example and the testing frequency band is from 0.2 GHz to 19 GHz, with incident angle $\theta_i = 0^\circ$, $\varphi_i = 0^\circ$. The structure is described in Fig. 6 of [8]. The geometric parameters of dielectric, as shown in Fig. 1, are $L = 1$, $l = 0$, $\varepsilon_{r1} = 4.33$, $h_1 = 1.6$ mm. The eight-legged element is discretized with 78 triangles resulting in 93 current unknown coefficients. Fig. 6 shows the comparison of the transmission coefficients between the direct MoM, one-dimensional ASM and experimental results given by [8]. Excellent agreement between the results of direct MoM, one-dimensional ASM and results in Ref. [8] has been achieved. The direct MoM responses are smoothed with 188 sampling points of equal space, whereas the responses of the ASM are interpolated by a single rational function obtained only by 27 MoM simulation samples. The CPU time to obtain accurate results is 1.2 CPU hours for direct MoM calculation and 0.3 CPU hours for ASM calculation, respectively.

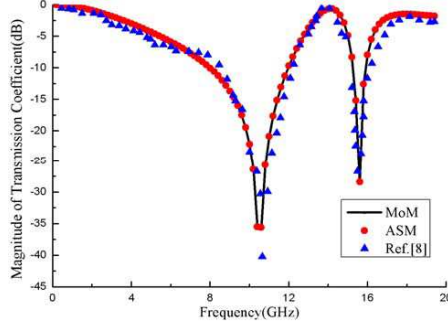


Figure 6. Frequency response of the eight-legged array.

4.2. The Patch-type Cross Element FSS

The reflection characteristic of the cross patch array, as shown in Fig. 5(a), is investigated under 21 GHz TE-polarization incident wave with incident angle changing. The testing ranges of θ_i and φ_i are from 1° to 81° and from 0° to 45° , respectively. The geometric parameters are presented as follow: $L_d = 6$ mm, $L_w = 1$ mm, $T_x = T_y = 8$ mm, $L = 3$, $l = 0$, $\varepsilon_{r1} = \varepsilon_{r3} = 3$, $\varepsilon_{r2} = 1$, $h_1 = h_3 = 0.2$ mm, $h_2 = 10$ mm. The induced current on the conductor of FSS cell is expanded by 64 RWG basic functions. Fig. 7 shows the comparison of the reflection coefficients between the direct MoM and the multi-dimensional ASM at $\varphi_i = 6^\circ$, 16° and 36° . As seen, the model of ASM simulation is in very good agreement with the MoM simulated result. The direct MoM responses are smoothed with 80×40 sampling points of equal space, whereas 31×17 sampling points are chosen in interpolation by the multi-dimensional ASM. It has to perform a simulation requiring 17 CPU hours by direct MoM. The proposed method computes the same information in less than 3 CPU hours.

The behavior of error convergence of the one-dimensional ASM modeling for the eight-legged array and the multi-dimensional ASM modeling for the cross patch array are given in Fig. 8. With the increase of the number of samples, two approximate models are close to the desired curves as much as expected, hence, the convergence of ASM is guaranteed.

4.3. The Aperture-type Ring Element FSS

A bivariate model was determined with ASM for the reflection characteristic of the aperture-type ring array as a function of the average radius (r) of ring and the thickness (h_1) of dielectric slab,

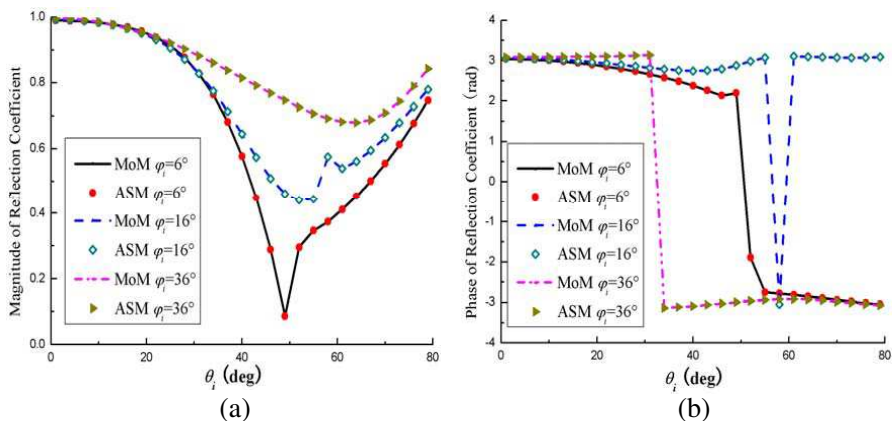


Figure 7. Reflection coefficient of the cross patch array as a function of incident angle. (a) Magnitude of reflection coefficient. (b) Phase of reflection coefficient.

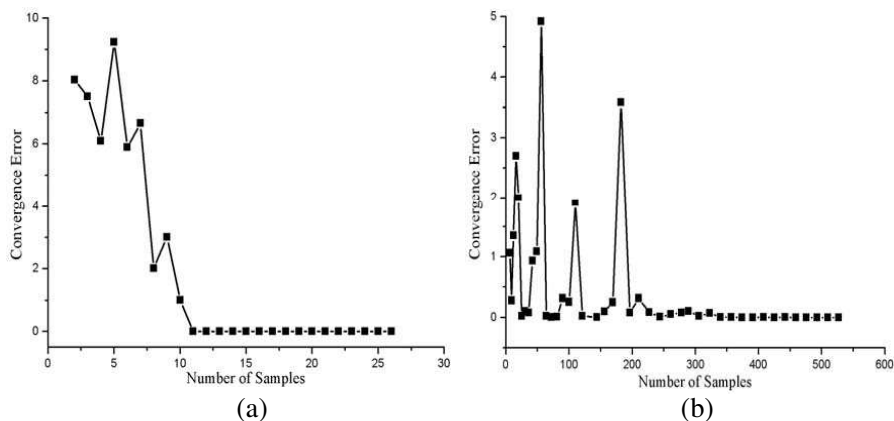


Figure 8. Convergence error. (a) One-dimensional ASM for the eight-legged array. (b) Two-dimensional ASM for the cross patch array.

as shown in Fig. 9. The geometric parameters of FSS cell, as shown in Fig. 5(b), are $w_r = 0.3$ mm, $T_x = T_y = 7.24$ mm. The geometric parameters of dielectric are $L = 1$, $l = 0$, $\epsilon_{r1} = 4$. The FSS is illuminated by an 11 GHz normal incident wave. The model is determined for the average radius $r \in [2.2, 3.2]$ and the thickness of dielectric slab $h_1 \in [6, 10]$ (unite: mm), which define the interpolation space. At initialization, the 20^2 equispaced grid points are chosen as testing points. Finally, the 8^2 sampling points are chosen and it costs

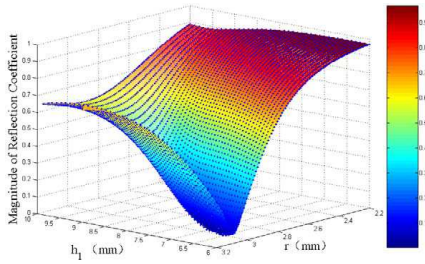


Figure 9. Reflection coefficient of the ring array as a function of h_1 and r .

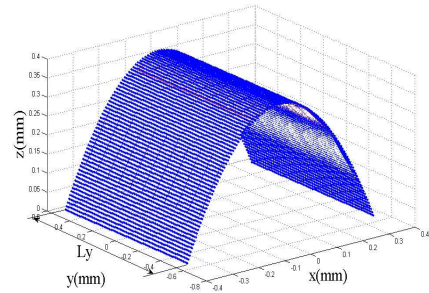


Figure 10. Model of FSS radome.

0.4 hours to calculate accurate results. Obtaining the same information by direct MoM, it requires 15 hours to perform a simulation.

4.4. The FSS Radome

The FSS Radome in design is a periodic array with aperture-type ring element mounted on a parabolic cylindrical surface, as shown in Fig. 10. The FSS cells are arranged periodically along the cross-sectional generatrix and y -axes, respectively. The cross section of FSS radome is parabola, which can be expressed as $x^2 = -a(z - h_z)$. h_z is the distance from top of radome to the origin of coordinates along z -axes. L_y is defined as the length of radome along y -axes. The parameters of radome are $a = 12\lambda$, $h_z = 12\lambda$, $L_y = 36\lambda$. λ is wavelength in free space. The rectangular aperture antenna with uniform distribution is selected and laid on the origin of coordinates.

4.4.1. Optimal Geometric Parameters Design of FSS

Using the model in Section 4.3, the geometric parameters r and h_1 of aperture-type ring element FSS have been optimized by particle swarm optimization with respect to the minimum magnitude of reflection coefficient at 11 GHz. The permittivity of dielectric slab is 4 and the tangent loss is 0.01. After 13 iterations, the optimization process is accomplished with the results of $r = 3$ mm, $h_1 = 6.68$ mm. The frequency response of the optimized FSS is shown in Fig. 11 and compared with the response of different r and h_1 with const h_1 and r , respectively. The multi-dimensional ASM solves the problem within 0.4 CPU hours. If using the direct MoM, the design of FSS geometric

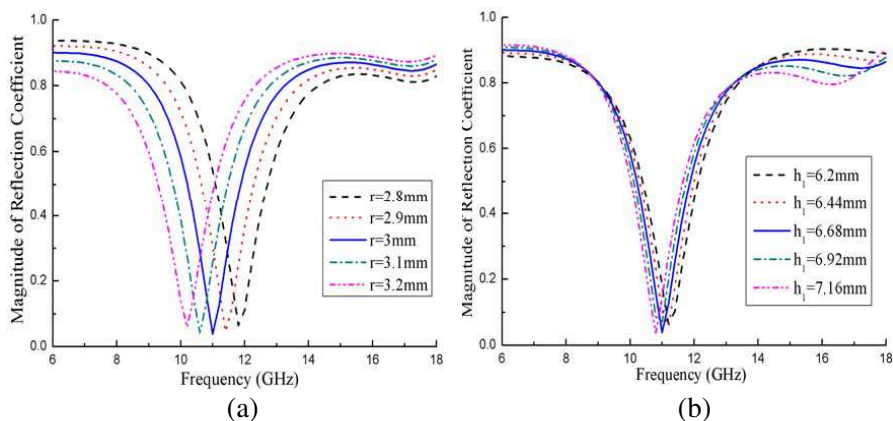


Figure 11. Frequency response of FSS (a) with const $h_1 = 6.68$ mm, (b) with const $r = 3$ mm.

parameters would cost much more effort for repeated computation on a very fine increment.

4.4.2. Pattern and Power Transmission of FSS Radome

The pattern of the radome enclosed antenna is evaluated by calculating the reaction between the field propagating through the selective radome and the equivalent currents on the antenna aperture. In the computation of the transmitted field, the curved frequency selective structure is replaced by the locally planar one which is tangent at the incidence point. The ASM is applied to efficiently derive the transmission coefficients of FSS under different incident angles, which is similar to the description in Section 4.2. The high-order Floquet modes of FSS effect have been ignored throughout.

The aperture-type ring element FSS, as selected in Section 4.4.1, is applied in FSS radome, which contains 132×135 ring cells. Fig. 12 shows that the radiation of the antenna is simulated individually when the FSS radome is presented or not. The scan angle of the antenna is assumed to be 0° . The operating frequency is 11 GHz. The transmitted field of curved FSS is evaluated separately by direct MoM and the ASM. Fig. 13 gives a quantitative description to present the relative error of the transmitted field at different locations of FSS radome obtained by the direct MoM and by the ASM, respectively. It is easy to found that a great agreement have archived. The maximum relative error for TE- and TM-polarization are below 0.2% and 0.8%, and the mean square deviations are 0.02% and 0.037%, which can satisfy the

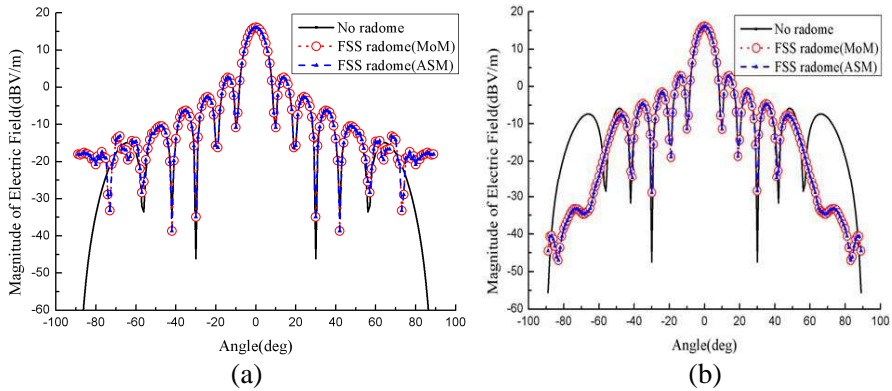


Figure 12. Pattern of FSS radome enclosed antenna. (a) *E*-plane. (b) *H*-plane. The pattern of antenna without radomes is also plotted for reference.

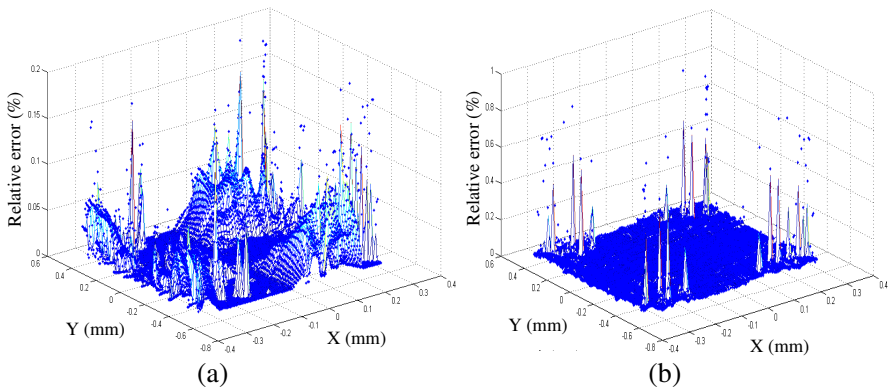


Figure 13. Relative error of the transmitted field obtained by the multi-dimensional ASM. (a) TE-polarization. (b) TM-polarization.

engineering demand. It requires 111.9 CPU hours for direct MoM simulation, whereas it only needs less than 0.8 CPU hours to compute the same information by the ASM. It seems that the ASM can save over 90% of extra computation effort.

The computation time for the direct MoM simulation of FSS radome is related to the number of FSS cells on the radome. However, during the ASM process, the cost of evaluating one interpolation grows in proportion to the number of sampling points in each dimension, i.e., $O\left(\prod_{i=1}^n K_i\right)$ and have nothing to do with the number of FSS cells. There

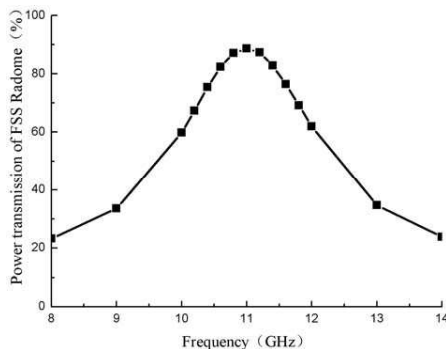


Figure 14. Power transmission of FSS radome.

are thousands of FSS cells on the radome for engineering project. Some performance of large FSS radome, such as the frequency response, scan angle of antennas and radar scattering cross section, should be considered that is unfeasible by the direct MoM. Fig. 14 gives the behavior of the power transmission of FSS radome from 8 GHz to 14 GHz through applying the ASM. At frequency 11 GHz, which is in the pass-band of the FSS radome, the maximum power transmission is archived 89%. It is verified that the FSS radome in design has a desired band-pass response and is prospectively useful for out-of-band RCS control. It costs 10.6 CPU hours by the ASM to obtain frequency response of FSS radome. Theoretically, it will require 1678.5 CPU hours for direct MoM simulation.

5. CONCLUSIONS

A fast adaptive sampling method to build multivariate rational function model for analysis and design of FSS is proposed. Since the proposed approach is based on the S-B algorithm which provides a great flexibility to construct various models of rational functions, the required model of rational function can be derived in an adaptive manner with the rapid convergence. Using the proposed approach, the response of FSS as function of incident frequency, incident direction and geometry dimensions of FSS can be modeled by one rational function with quite less number of sampling points of MoM calculation. The algorithm can be applicable in a very broad rang and does not require any a priori knowledge of FSS.

Various models were built for FSS with different shape elements and FSS radome to verify the propose approach. The results using multi-dimensional ASM compare very well to electromagnetic

simulation by the direct MoM. The proposed method offers tremendous computational savings in terms of CPU time that makes it possible to analyze and design FSS with arbitrary element more efficiently, especially for the large FSS radome in engineering project.

ACKNOWLEDGMENT

This work is supported by the Doctorate Foundation of Northwestern Polytechnical University (Grant No. CX201115) and by Science Foundation of Aeronautics (Grant No. 20101853019).

REFERENCES

1. Zappelli, L., "Modified dielectric frequency selective surfaces with enlarged bandwidth and angular stability," *IEEE Trans. on Antennas and Propagat.*, Vol. 59, No. 10, 3668–3678, 2011.
2. Xue, J.-Y., S.-X. Gong, P.-F. Zhang, W. Wang, and F.-F. Zhang, "A new miniaturized fractal frequency selective surface with excellent angular stability," *Progress In Electromagnetics Research Letters*, Vol. 13, 131–138, 2010.
3. Robert, A. K. and C. H. Chan, "A numerically efficient technique for the method of moments solution for planar periodic structures in layered media," *IEEE Trans. Microwave Theory and Techniques*, Vol. 42, No. 4, 635–643, 1994.
4. Rao, S. M., D. R. Wilton, and A. W. Glisson, "Electromagnetic scattering by surface of arbitrary shape," *IEEE Trans. on Antennas and Propagat.*, Vol. 30, No. 3, 409–418, 1982.
5. Chan, C. H. and R. Mittra, "On the analysis of frequency selective surface using subdomain basis functions," *IEEE Trans. on Antennas and Propagat.*, Vol. 38, No. 1, 40–50, 1990.
6. Chun, Y. and C. C. Lu, "Analysis of finite and curved frequency-selective surfaces using the hybrid volume-surface integral equation approach," *Microwave and optical technology letters*, Vol. 45, No. 2, 107–112, 2005.
7. Martini, E., F. Caminita, M. Nannetti, et al., "Fast analysis of FSS radome for antenna RCS reduction," *IEEE Antennas and Propagation Society International Symposium*, 1801–1804, 2006.
8. Hajlaoui, E. A., H. Trabelsi, et al., "Analysis of novel dual-resonant and dual-polarized frequency selective surface using periodic contribution of wave concept iterative process PPMS-WCIP," *3rd International Conference on Information and*

- Communication Technologies: From Theory to Applications*, 1–6, 2008.
9. Mittra, R., C. H. Chen, and T. A. Cwick, “Techniques for analyzing frequency selective surfaces—a review,” *Proceedings of IEEE*, Vol. 76, No. 12, 1593–1615, 1988.
 10. Reddy, C. J., M. D. Deshpande, C. R. Cockrell, et al., “Fast RCS computation over a frequency band using method of moments in conjunction with asymptotic waveform evaluation technique,” *IEEE Trans. on Antennas and Propagat.*, Vol. 46, 1229–1233, 1998.
 11. Chen, M. S., Q. Wu, et al., “A new approach for fast solution of electromagnetic scattering problems over a broad frequency band,” *3rd IEEE International Symposium on Microwave, Antenna, Propagation and EMC Technologies for Wireless Communications*, 932–934, 2009.
 12. Ma, X., G. B. Wan, et al., “Efficient analysis of FSS using the MoM-based Maehly approximation,” *Proceedings of 2011 Cross Strait Quad-regional Radio Science and Wireless Technology Conference*, 21–24, 2011.
 13. Ding, Y., K. L. Wu, and D. G. Fang, “A broad-band adaptive-frequency-sampling approach for microwave-circuit EM simulation exploiting Stoer-Bulirsch algorithm,” *IEEE Transaction on Microwave Theory and Technique*, Vol. 51, No. 3, 928–934, 2003.
 14. Chen, J. Q., Z. W. Liu, and R. S. Chen, “An adaptive frequency sampling method for frequency selective surface design exploiting Steor-Bulirsch algorithm,” *Asia-Pacific Microwave Conference*, Bangkok, December 11–14, 2007.
 15. Lehmensiek, R. and P. Meyer, “Creating accurate multivariate rational interpolation of microwave circuits by using efficient adaptive sampling to minimize the number of analyses,” *IEEE Transaction on Microwave Theory and Technique*, Vol. 49, No. 8, 1419–1430, 2001.
 16. Geest, J. D., T. Dhaene, N. Faché, and D. De Zutter, “Adaptive CAD-model building algorithm for general planar microwave structures,” *IEEE Transactions on Microwave Theory and Techniques*, Vol. 47, No. 9, 1801–1809, 1999.
 17. Peik, S. F., R. R. Mansour, and Y. L. Chow, “Multidimensional cauchy method and adaptive sampling for and accurate microwave circuit modeling,” *IEEE Transaction on Microwave Theory and Technique*, Vol. 46, No. 12, 2364–2371, 1998.
 18. Wu, T. K., *Frequency Selective Surface and Grid Array*, John Wiley & Sons, New York, 1995.

19. McInturff, K. and P. S. Simon, "The Fourier transform of linearly varying functions with polygonal support," *IEEE Trans. on Antennas and Propagat.*, Vol. 39, No. 9, 1441–1443, 1991.
20. Stoer, J. and R. Bulirsch, *Introduction to numerical analysis*, Springer-Verlag, Berlin, 1980.